



Libraries and Learning Services

# University of Auckland Research Repository, ResearchSpace

## Version

This is the Accepted Manuscript version. This version is defined in the NISO recommended practice RP-8-2008 <http://www.niso.org/publications/rp/>

## Suggested Reference

Price, L. C., Peiris, H. V., Frazer, J., & Easter, R. (2015). Gravitational wave consistency relations for multifield inflation. *Physical Review Letters*, 114(3), 031301-1-031301-6.

doi: [10.1103/PhysRevLett.114.031301](https://doi.org/10.1103/PhysRevLett.114.031301)

## Copyright

This is an open-access article distributed under the terms of the [Creative Commons Attribution](https://creativecommons.org/licenses/by/4.0/) License.

Items in ResearchSpace are protected by copyright, with all rights reserved, unless otherwise indicated. Previously published items are made available in accordance with the copyright policy of the publisher.

<http://journals.aps.org/authors/open-access-physical-review-physical-review-letters>

<http://www.sherpa.ac.uk/romeo/issn/0031-9007/>

<https://researchspace.auckland.ac.nz/docs/uoa-docs/rights.htm>

# Gravitational wave consistency relations for multifield inflation

Layne C. Price,<sup>1,\*</sup> Hiranya V. Peiris,<sup>2,†</sup> Jonathan Frazer,<sup>3,‡</sup> and Richard Easther<sup>1,§</sup>

<sup>1</sup>*Department of Physics, University of Auckland, Private Bag 92019, Auckland, New Zealand*

<sup>2</sup>*Department of Physics and Astronomy, University College London, London WC1E 6BT, U.K.*

<sup>3</sup>*Department of Theoretical Physics, University of the Basque Country UPV/EHU, 48040 Bilbao, Spain*  
(Dated: December 23, 2014)

We study the tensor spectral index  $n_t$  and the tensor-to-scalar ratio  $r$  in the simplest multifield extension to single-field, slow-roll inflation models. We show that multifield models with potentials  $V \sim \sum_i \lambda_i |\phi_i|^p$  have different predictions for  $n_t/r$  than single-field models, even when all the couplings are equal  $\lambda_i = \lambda_j$ , due to the probabilistic nature of the fields' initial values. We analyze well-motivated prior probabilities for the  $\lambda_i$  and initial conditions to make detailed predictions for the marginalized probability distribution of  $n_t/r$ . With  $\mathcal{O}(100)$  fields and  $p > 3/4$ , we find that  $n_t/r$  differs from the single-field result of  $n_t/r = -1/8$  at the  $5\sigma$  level. This gives a novel and testable prediction for the simplest multifield inflation models.

A cosmological gravitational wave background (CGWB) is a compelling signature of inflation, which is already supported by the highly Gaussian primordial perturbations [1, 2] and their broken scale invariance, now detected at  $5\sigma$  significance [3, 4]. A large-amplitude CGWB provides fundamentally new tests of single-field slow-roll (SFSR) inflation via the *consistency relation* [5]  $n_t/r = -1/8$ , which relates the tensor spectral index  $n_t$  to the ratio of the tensor and scalar perturbation amplitudes,  $r$ .

While there has been dramatic progress towards the direct detection of a CGWB through the  $B$ -mode polarization in the cosmic microwave background (CMB) [6], measuring  $n_t$  is challenging with current technologies [7–9]. However, for  $r \gtrsim 0.1$  this will be feasible with the next generation of space-based [10, 11], ground-based [12–15], and balloon-borne [16, 17] experiments, while future 21 cm projects [18, 19] could also detect lensing by a CGWB and direct detection experiments [20, 21] would test the consistency condition using the lever arm between CMB and solar system scales to far greater accuracy with  $r \gtrsim \mathcal{O}(10^{-3})$ .

The simplest inflationary scenarios that yield an easily detectable CGWB are *monomial* models with the inflationary potential  $V \sim |\phi|^p$ , which have  $0.05 \lesssim r \lesssim 0.30$  for  $2/3 \lesssim p \lesssim 4$ . Single field models are *simple* but not necessarily *natural*, as many high energy theories yield large numbers of scalar degrees of freedom [22–25]. For multifield models the consistency relation is reduced to an inequality,  $n_t/r \leq -1/8$ . While  $r$  and  $n_t$  are correlated for  $N_f = 2$  [26, 27], there is no known relationship between  $r$  and  $n_t$  when  $N_f$  is large.

In this *Letter*, we derive a robust prediction for  $n_t/r$  for  $N_f$ -*monomial* models, with potential

$$V = \frac{1}{p} \sum_i \lambda_i |\phi_i|^p, \quad (1)$$

where  $\lambda_i$  are real, positive constants and summations run over the number of fields,  $N_f$ . Eq. (1) arises naturally

in many high energy theories [28–35] and is a simple, intuitive generalization of the chaotic SFSR models.

We treat the  $\lambda_i$  and the values of  $\phi_i$  at a fixed number of  $e$ -folds before the end of inflation as independent random variables. When  $N_f \rightarrow \infty$ , the central limit theorem ensures that  $n_t/r$  is a Gaussian random variable. Critically,  $\langle n_t/r \rangle$  does not reduce to the single-field limit if the couplings are identical unless the field values  $\phi_{i,*}$  when the pivot scale  $k_*$  leaves the horizon are also fixed, except for the special case  $p = 2$ . The expected value of  $n_t/r$  depends only on two moments of the distributions of the  $\lambda_i$  and  $\phi_i$ , and is independent of  $N_f$ . The variance in  $n_t/r$  is  $s_{n_t/r}^2 \sim 1/N_f$  (for  $p > 3/4$ ), giving a sharp, generic prediction for the consistency relation in the many-field limit. This provides a direct test for distinguishing between  $N_f$ -monomial models and their single-field analogues.

**Model**— In some cases the  $\lambda_i$  in Eq. (1) might be derivable from fundamental theory, but in general we are ignorant of their values, so we treat these terms as independent random variables (RVs) with a prior probability  $P(\lambda)$ . Similarly, we do not know the fields' initial conditions, so we also treat these as identically distributed, but possibly correlated, RVs with a prior probability  $P(\phi_0)$ . We then marginalize over the  $P(\lambda)$  and  $P(\phi_0)$  to produce a probability distribution for  $n_t/r$ . Since a change of variables  $\phi_i \rightarrow \tilde{\phi}_i(\phi_j, \lambda_j)$  will mix the  $\lambda_i$  and  $\phi_i$ , it is clear that there is no *a priori* difference between these two types of parameters, motivating our statistical approach.

The simplest choice for  $P(\phi_0)$  is a uniform distribution of  $\phi_{i,*}$  defined when the pivot scale  $k_*$  leaves the horizon  $N_*$   $e$ -folds before the end of inflation. This choice contains the least Shannon information about the fields' initial states and ensures that most of the fields are dynamically relevant. Further, this  $P(\phi_0)$  and others were extensively studied in Ref. [36], where it was shown that the initial conditions only weakly affect the predicted density spectra. The likely values of  $n_s$  and  $r$  for a related class of multifield monodromy models was derived in Ref. [37],

finding  $0.955 \lesssim n_s \lesssim 0.975$ . Furthermore,  $r = 4p/N_*$ , and the non-Gaussianity is small.

**$\delta N$  formalism**— The potential in Eq. (1) is sum-separable and, assuming slow-roll,  $N_*$  is [38, 39]

$$N_* = - \int_*^c \sum_i \frac{V_i}{V'_i} d\phi_i, \quad (2)$$

where  $V'_i = \lambda_i |\phi_i|^{p-1}$  and  $\phi_{i,*}$  and  $\phi_{i,c}$  denote field values at horizon crossing and the end of inflation, respectively. For  $N_f$ -monomial inflation

$$N_* = \frac{1}{2p} \sum_i [\phi_{i,*}^2 - \phi_{i,c}^2]. \quad (3)$$

The  $\delta N$  formalism relates the field perturbations at horizon crossing to the gauge-invariant curvature perturbation  $\zeta$  on constant density hypersurfaces via

$$\zeta \approx \sum_i N_{*,i} \delta\phi_{i,*}, \quad (4)$$

where  $N_{*,i} \equiv \partial N_*/\partial\phi_{i,*}$ . If the field perturbations are well-approximated by a free field theory with power spectrum  $\mathcal{P}_{\delta\phi}^{ij} = (H_*/2\pi)^2 \delta^{ij}$  at horizon crossing, the tensor-to-scalar ratio is

$$r = \frac{8}{\sum_i N_{*,i} N_{*,i}}. \quad (5)$$

To first-order in slow-roll  $n_t = -2\epsilon$ , where

$$\epsilon = \frac{1}{2} \sum_i \left[ \frac{V'_i}{V} \right]^2. \quad (6)$$

For  $N_f$ -monomial models, the field values  $\phi_{i,c}$  at the end of inflation can typically be neglected. This *horizon crossing approximation* (HCA) (e.g., Refs. [38, 40]) is a simplification of the  $\delta N$  formalism that incorporates the super-horizon evolution of  $\zeta$ , but ignores quantities contributing to  $N_*$  from the end-of-inflation surface. Setting  $\phi_{i,c} \rightarrow 0$  in Eq. (3), we find

$$\frac{n_t}{r} = -\frac{1}{4p^2} \epsilon \sum_i \phi_{i,*}^2, \quad (7)$$

where we restrict our attention to cases that are slowly rolling at horizon crossing. Requiring  $\epsilon \lesssim 0.1$  then sets the maximum deviation from the single-field result as

$$-\left(\frac{N_*}{2p}\right) \times \mathcal{O}(10^{-1}) \lesssim \frac{n_t}{r} \leq -\frac{1}{8}. \quad (8)$$

**The many-field limit**— We build the probability distribution for  $n_t/r$  by marginalizing Eq. (7) over  $P(\phi_0)$  and  $P(\lambda)$ , and use the central limit theorem (CLT) to take the large  $N_f$  limit,  $N_f \rightarrow \infty$ . By Eq. (3) the HCA implies that  $P(\phi_0)$  is a uniform distribution pulled back onto an  $N_f$ -sphere in field-space with radius  $\sqrt{2pN_*}$ .

Since the multivariate normal distribution  $\vec{x} \sim \mathcal{N}(0, \mathbb{1})$  is invariant under rotations of  $\vec{x}$ , we can sample this  $N_f$ -sphere uniformly by defining

$$\phi_{i,*} = \sqrt{\frac{2pN_*}{\sum_j x_j^2}} x_i \quad \text{for } \vec{x} \sim \mathcal{N}(0, \mathbb{1}). \quad (9)$$

Using Eq. (9), the summations in Eqs. (6) and (7) are

$$\sum_i \lambda_i^n |\phi_{i,*}|^m = \sum_i \lambda_i^n \left[ \frac{2pN_*}{\sum_j x_j^2} \right]^{\frac{m}{2}} |x_i|^m. \quad (10)$$

As  $N_f \rightarrow \infty$  the CLT shows that the numerator is normally distributed with mean

$$\mu_{\text{num}} = N_f (2pN_*)^{m/2} \langle \lambda^n \rangle \langle |x|^m \rangle \quad (11)$$

and standard deviation

$$s_{\text{num}} = \sqrt{N_f} (2pN_*)^{m/2} \sigma_{n,m}, \quad (12)$$

where  $\langle \cdot \rangle$  indicates expected value and

$$\sigma_{n,m}^2 \equiv \langle \lambda^{2n} \rangle \langle |x|^{2m} \rangle - \langle \lambda^n \rangle^2 \langle |x|^m \rangle^2, \quad (13)$$

which assumes that the  $\lambda_i$  and  $x_j$  are independent. Finally, the denominator in Eq. (9) is drawn from the  $\chi$ -distribution, which is closely approximated by  $\mathcal{N}(\sqrt{N_f}, 1/\sqrt{2})$  for  $x_i \sim \mathcal{N}(0, 1)$ .

The numerator and denominator in Eq. (10) are correlated by the constraint in Eq. (3). For a given variance in  $P(\lambda)$ , the correlation  $\gamma$  is maximized when  $m = 2$  and  $|\gamma| \rightarrow 1$  as the variance vanishes. Since each  $\sum_i \lambda_i^n |\phi_{i,*}|^m$  is uniquely determined given  $\vec{\lambda}$  and  $\vec{\phi}_*$ , we expect a strong correlation between the numerator and denominator in Eq. (6) for typical choices of  $P(\lambda)$ . This significantly reduces the variance of  $n_t/r$ , and ensures a sharp prediction for its value. We numerically calculate  $\gamma$  after defining the priors on  $\lambda$ .

For any normally distributed variable  $y \sim \mathcal{N}(\mu, \sigma)$

$$\langle |y|^m \rangle = \frac{2^{\frac{m}{2}} \sigma^m}{\sqrt{\pi}} \Gamma\left(\frac{1+m}{2}\right) F_{1,1}\left(\frac{-m}{2}; \frac{1}{2}; \frac{-\mu^2}{2\sigma^2}\right), \quad (14)$$

for  $m > -1$ , and  $F_{1,1}$  is the confluent hypergeometric function of the first kind. If  $\mu = 0$ , as for  $x_i \sim \mathcal{N}(0, 1)$ , then  $F_{1,1} = 1$  and only the  $\Gamma$  function contributes to the moments.

If  $m < -1$ ,  $\langle |y|^m \rangle$  may diverge if  $P(y = 0)$  does not vanish fast enough. This is indeed the case for  $x_i \sim \mathcal{N}(0, 1)$ , and we cannot predict the distribution of the sums in Eq. (10) with  $m \leq -1$ . Sums like Eq. (10) are effectively finite numerical approximations to the integral

$$\frac{1}{N_f} \sum_i \lambda_i^n |x_i|^m \approx \int |x|^m \mathcal{N}(0, 1) dx \int \lambda^n P(\lambda) d\lambda, \quad (15)$$

which diverges for  $m < -1$ . While ratios of these sums might be well-defined [41], our approach shows that a finite prediction for both the mean and the standard deviation of  $n_t/r$  requires  $p > 3/4$ , while only requiring a finite mean needs  $p > 1/2$ , using the CLT.

**The method**— Since  $n_t/r$  is given by Eq. (7) and the sums in Eq. (10) are ratios of correlated, normally distributed RVs, the key tool for this analysis is the ratio distribution  $f_{\text{ratio}}(\alpha/\beta)$  for normally distributed RVs  $\alpha$  and  $\beta$ . If  $w \equiv \alpha/\beta$ , then as  $P(\beta > 0) \rightarrow 1$  the CDF for the ratio distribution  $f_{\text{ratio}}(w)$  is approximately [42]

$$F_{\text{ratio}}(w) = \Phi \left[ \frac{\mu_\beta w - \mu_\alpha}{\sigma_\alpha \sigma_\beta a(w)} \right], \quad (16)$$

where  $\mu_i$  and  $\sigma_i^2$  are the respective means and variances,

$$a(w) \equiv \left[ \frac{w^2}{\sigma_\alpha^2} - \frac{2\gamma w}{\sigma_\alpha \sigma_\beta} + \frac{1}{\sigma_\beta^2} \right]^{1/2}, \quad (17)$$

and

$$\Phi(z) \equiv \frac{1}{2} \left[ 1 + \text{Erf} \left( \frac{z}{\sqrt{2}} \right) \right] \quad (18)$$

for real  $z$ . When  $N_f$  is large,  $f_{\text{ratio}}$  approaches a normal distribution with mean  $\mu_\alpha/\mu_\beta$  and standard deviation

$$s = \frac{\sqrt{\mu_\beta^2 \sigma_\alpha^2 - 2\gamma \mu_\alpha \mu_\beta \sigma_\alpha \sigma_\beta + \mu_\alpha^2 \sigma_\beta^2}}{\mu_\beta^2}. \quad (19)$$

The mean of  $f_{\text{ratio}}$  is independent of the correlations  $\gamma$ , and the standard deviation for  $n_t/r$  is a straightforward — but messy — algebraic function of  $\langle \lambda \rangle$ ,  $\langle \lambda^2 \rangle$ , and  $\langle \lambda^4 \rangle$ , as well as  $\langle |x|^m \rangle$  for  $m = 2, 4, p, 2p, 2p-2$ , and  $4p-4$ .

To obtain the distribution  $f_{\text{ratio}}(n_t/r)$  we express the consistency relation in terms of the sums in Eq. (10) as

$$\frac{n_t}{r} = -\frac{pN_*}{4} \left[ \frac{\sum_i \lambda_i^2 |\phi_{i,*}|^{2p-2}}{\left( \sum_j \lambda_j |\phi_{j,*}|^p \right)^2} \right]. \quad (20)$$

For each sum above, we calculate the covariance in Eq. (10) between the numerator and denominator given  $P(\lambda)$ , and use Eq. (19) to find the variance of the sum. Although the denominator  $(\sum_i \lambda_i |\phi_{i,*}|^p)^2$  is then  $\chi^2$ -distributed, this is approximately normal in the many-field limit. We then substitute these two normally-distributed RVs back into Eq. (16). Similarly, we evaluate the correlation between the numerator and denominator in Eq. (20), finally obtaining the probability distribution for  $n_t/r$ .

**Novel multifield predictions**— From the ratio distribution (16), as  $N_f \rightarrow \infty$  the value of  $n_t/r$  in Eq. (20) is normally distributed with a mean

$$\left\langle \frac{n_t}{r} \right\rangle_{N_f \uparrow} = \left[ -\frac{1}{8} \right] \left[ \frac{\langle \lambda^2 \rangle}{\langle \lambda \rangle^2} \right] \left[ \frac{\sqrt{\pi} \Gamma(p - \frac{1}{2})}{2 \Gamma^2(\frac{p+1}{2})} \right] \quad (21)$$

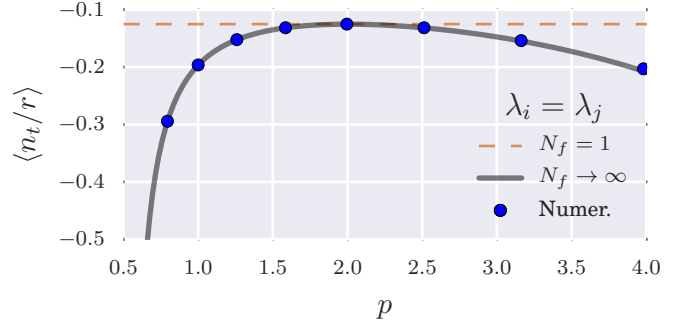


FIG. 1. The multifield prediction from Eq. (21) compared to the numerical mean  $\langle n_t/r \rangle$  of simulations with 5000 samples, at each plotted value of  $p$ , with  $N_f = 1000$  using the horizon-crossing approximation. The field values  $\phi_{i,*}$  as the pivot scale  $k_*$  leaves the horizon are drawn from a uniform prior on the surface in Eq. (3) and all the couplings  $\lambda_i$  are identical.

and a standard deviation proportional to

$$s_{n_t/r} \propto \frac{1}{\sqrt{N_f}} \rightarrow 0 \quad \text{as} \quad N_f \rightarrow \infty, \quad (22)$$

which can be found by substituting the means, variances, and correlations of Eq. (10) into Eq. (19).

The first bracketed term in Eq. (21) is the single-field prediction, the second is due to the couplings  $\lambda_i$ , and the third arises from the uniform prior for  $\phi_{i,*}$  on the horizon-crossing surface. This last term is due only to the spread in the field values at horizon crossing and is independent of everything except  $p$ . The functional form of this term is fixed by the uniform prior distribution on the horizon crossing surface, but other prior probabilities for  $\phi_{i,*}$  result in qualitatively similar behavior as demonstrated in Ref. [36]. As Eq. (22) vanishes in the many-field limit, Eq. (21) is the generic multifield prediction, which deviates from the single-field result at  $> 5\sigma$  for  $N_f \gtrsim \mathcal{O}(10^2)$  for typical  $P(\lambda)$ .

Consequently, even if  $\langle \lambda^2 \rangle = \langle \lambda \rangle^2$ ,  $N_f$ -monomial models do not predict  $n_t/r = -1/8$ , unless the  $\phi_{i,*}$  are also identical. Fig. 1 compares the predicted value for  $\langle n_t/r \rangle$  in Eq. (21), with all  $\lambda_i$  equal, to numerical results obtained by directly evaluating  $n_t/r$  with Eq. (7), showing excellent agreement for many fields. The divergence at  $p = 1/2$  reflects the fact that  $\langle |x|^{2p-2} \rangle \rightarrow \infty$ . Thus, when  $p \leq 1/2$ ,  $\langle n_t/r \rangle$  may be arbitrarily large, which violates the slow-roll assumption. Consequently, these models are most easily distinguished from their single field analogues, but the hardest to make accurate predictions for.

**Specific examples**— To understand how the mean  $\langle n_t/r \rangle$  in Eq. (21) is affected by  $P(\lambda)$  we compare two explicit priors that are widely used in Bayesian analyses of inflation [4, 43–46]. We focus on the  $p = 2$  case, since the dependence on the prior on  $\phi_{i,*}$  in Eq. (21) cancels for this scenario.

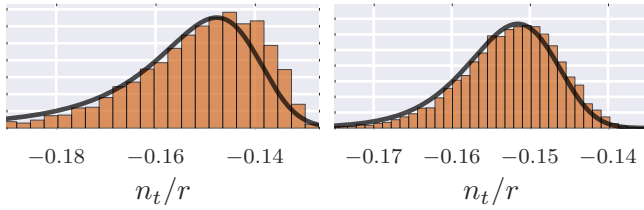


FIG. 2. Predicted probability distributions for  $n_t/r$  with  $p = 2$  compared with histograms built from 10000 numerical samples. The couplings  $\lambda_i$  are drawn from the Uniform Model with (left)  $N_f = 20$  and (right)  $N_f = 100$ . For  $N_f \lesssim \mathcal{O}(10^2)$ , the distribution is skewed toward positive values as predicted.

We look at two cases: uniform prior probabilities over  $\lambda_i$  or  $\alpha_i$  for  $\lambda_i \equiv 10^{\alpha_i}$ , which we denote the *Uniform Model* and *Log Model*, respectively. The Uniform Model would be applicable when the relevant scale of  $\lambda_i$  is known to within an order of magnitude, while the Log Model effectively scans over a range of physical scales.

For the Uniform Model, the  $\lambda_i$  are drawn from  $\mathcal{U}[a, b]$ , and Eq. (21) becomes

$$\left(\frac{n_t}{r}\right)_{p=2}^{\text{unif}} = -\frac{1}{6} \left[ \frac{b^2 + ab + a^2}{(b+a)^2} \right]. \quad (23)$$

For  $\lambda_i \in [10^{-14}, 10^{-13}]$ , as  $N_f \rightarrow \infty$  the predicted correlation coefficient for  $f_{\text{ratio}}(n_t/r)$  is  $\gamma \approx -0.98$  and  $\langle n_t/r \rangle = -0.153$ . We plot  $f_{\text{ratio}}$  and the results of 10000 numerical realizations using the HCA in Fig. 2. We find excellent agreement with Eq. (23), with  $f_{\text{ratio}}$  accurately capturing the higher order moments of the  $n_t/r$  distribution for  $N_f \gtrsim 20$ . For  $p = \{3/2, 2, 3\}$  the single-field result  $n_t/r = -1/8$  is a  $5\sigma$  deviation from the mean in Eq. (23) for  $N_f \gtrsim \{120, 120, 200\}$ , respectively.

For the Log Model with  $\alpha \sim \mathcal{U}[a, b]$ ,

$$\left(\frac{n_t}{r}\right)_{p=2}^{\text{log}} = -\frac{\log(10)(b-a)}{16} \left[ \frac{10^b + 10^a}{10^b - 10^a} \right]. \quad (24)$$

If  $a \rightarrow b$ , we recover the single-field result in both Eqs. (23) and (24). However, Eq. (24) diverges as  $a \rightarrow -\infty$ , reflecting the failure of slow-roll in the limit of widely separated scales. For  $\alpha \in [-14, -12]$  the Log Model predicts  $\mathcal{P}_\zeta \sim \mathcal{O}(10^{-9})$ ,  $\epsilon \lesssim 0.03$ ,  $\gamma \approx -0.95$  and  $n_t/r = -0.294$ . For  $p = \{3/2, 2, 3\}$  the single-field result is a  $5\sigma$  deviation from the mean in Eq. (24) for  $N_f \gtrsim \{145, 135, 255\}$ , respectively.

**Relaxing the approximations**— Fig. 3 compares the HCA prediction to numerical results that include the contribution from the end-of-inflation surface in Eq. (3), with  $\phi_{i,c} \neq 0$ . We numerically solve the background Klein-Gordon equations for 1000 realizations, finding the field values at the end of inflation (defined by  $\epsilon = 1$ ) and obtaining the full  $\delta N$  prediction without using the HCA. Fig. 3 also incorporates both the sub-horizon evolution of the modes and any non-slow-roll behavior by solving

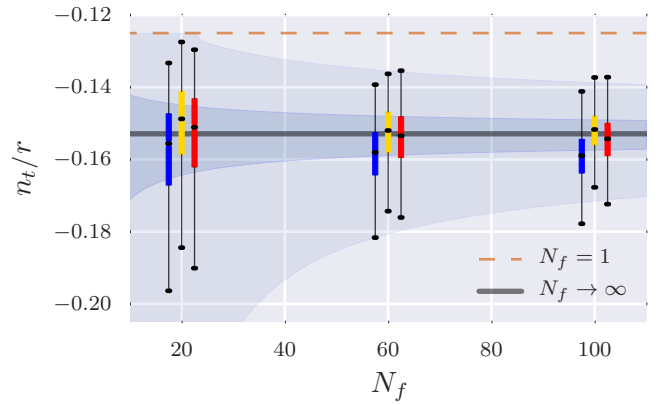


FIG. 3. The consistency relation for the Uniform Model with  $p = 2$  is plotted for different  $N_f$ , marginalizing over initial field values. The boxes/whiskers cover the 50/97% CIs and the gray regions delineate the same ranges as predicted by the HCA and the central limit theorem. The (dashed) brown and (solid) gray lines are the single-field and the many-field HCA predictions, respectively. For each case we present results derived from full numerical solutions to the mode equations (blue/left), the slow-roll prediction using the HCA (yellow/center), and the slow-roll prediction including the end-of-inflation surface (red/right) for  $N_f = 20, 60$ , and  $100$ .

the mode equations numerically, as in Refs. [36, 47], using MULTIMODECODE [48]. Results are plotted for the Uniform Model, with the ranges  $\lambda_i \in [10^{-14}, 10^{-13}]$  and  $p = 2$ .

In all cases the numerical results are well-approximated by the HCA. The HCA results are marginally larger than the numerical results, which we attribute to second-order corrections to the slow-roll equations;  $n_t = -2\epsilon/(1-\epsilon)$ , which suppresses  $n_t$  relative to the first-order approximation. The variances in the numerical results scale as  $\sigma^2 \propto 1/\sqrt{N_f}$ , as predicted by the HCA results, confirming that many-field models make sharp predictions for  $n_t/r$ .

**Conclusion**— We have computed the probability distribution for the consistency relation  $n_t/r$  for inflation driven by multiple scalar fields with monomial potential terms, as a function of the distribution of couplings and initial field values. The single-field result is clearly distinguishable from the many-field limit, providing a clean and compelling signature that distinguishes these models from their single-field analogues. Other than for the quadratic case, this result holds even when the couplings are identical.

We focused on computing the slow roll parameter  $\epsilon$ , but the nature of the slow-roll hierarchy [49] indicates that this approach will generalize to a variety of observables, so quantities such as  $f_{\text{NL}}$  that rely on the second and higher slow-roll parameters should also have precise predictions that deviate from the single-field expectation even when the couplings are degenerate. This provides a further compelling example of a multifield scenario in



which the observables have a sharp and *generic* prediction in the many-field limit [32, 34–36, 40, 41, 50–57].

The expected value  $\langle n_t/r \rangle$  depends on only two moments of the prior probability distributions  $P(\lambda)$  and  $P(\phi_0)$ , and the corresponding variance is  $s_{n_t/r}^2 \propto 1/N_f$ . The single-field expectation of  $n_t/r = -1/8$  differs from the multifield result at the  $5\sigma$  level when  $N_f \gtrsim \mathcal{O}(10^2)$ . Consequently, given specific priors for the field values and couplings, we obtain generic and testable predictions for the consistency relations in this large and interesting class of multifield inflation models.

*Acknowledgments*— We thank Grigor Aslanyan, Andrew Jaffe, and Jonathan White for helpful discussions. HVP is supported by STFC and the European Research Council under the European Community’s Seventh Framework Programme (FP7/2007-2013) / ERC grant agreement no 306478-CosmicDawn. JF is supported by IKERBASQUE, the Basque Foundation for Science. We acknowledge the contribution of the NeSI high-performance computing facilities. New Zealand’s national facilities are provided by the New Zealand eScience Infrastructure (NeSI) and funded jointly by NeSI’s collaborator institutions and through the Ministry of Business, Innovation & Employment’s Research Infrastructure programme [58]. This work has been facilitated by the Royal Society under their International Exchanges Scheme. This work was supported in part by National Science Foundation Grant No. PHYS-1066293 and the hospitality of the Aspen Center for Physics.

---

\* [lpri691@aucklanduni.ac.nz](mailto:lpri691@aucklanduni.ac.nz)

† [h.peiris@ucl.ac.uk](mailto:h.peiris@ucl.ac.uk)

‡ [j.frazer@ucl.ac.uk](mailto:j.frazer@ucl.ac.uk)

§ [r.easter@auckland.ac.nz](mailto:r.easter@auckland.ac.nz)

- [1] P. Ade *et al.* (Planck Collaboration), (2013), [arXiv:1303.5084 \[astro-ph.CO\]](#).
- [2] B. Leistedt, H. V. Peiris, and N. Roth, (2014), [arXiv:1405.4315 \[astro-ph.CO\]](#).
- [3] P. Ade *et al.* (Planck Collaboration), *Astron.Astrophys.* (2014), 10.1051/0004-6361/201321591, [arXiv:1303.5076 \[astro-ph.CO\]](#).
- [4] P. Ade *et al.* (Planck Collaboration), (2013), [arXiv:1303.5082 \[astro-ph.CO\]](#).
- [5] E. J. Copeland, E. W. Kolb, A. R. Liddle, and J. E. Lidsey, *Phys.Rev.Lett.* **71**, 219 (1993), [arXiv:hep-ph/9304228 \[hep-ph\]](#).
- [6] P. Ade *et al.* (BICEP2 Collaboration), *Phys.Rev.Lett.* **112**, 241101 (2014), [arXiv:1403.3985 \[astro-ph.CO\]](#).
- [7] L. Verde, H. Peiris, and R. Jimenez, *JCAP* **0601**, 019 (2006), [arXiv:astro-ph/0506036 \[astro-ph\]](#).
- [8] S. Dodelson, *Phys.Rev.Lett.* **112**, 191301 (2014), [arXiv:1403.6310 \[astro-ph.CO\]](#).
- [9] J. Caligiuri and A. Kosowsky, *Phys.Rev.Lett.* **112**, 191302 (2014), [arXiv:1403.5324 \[astro-ph.CO\]](#).
- [10] D. Baumann *et al.* (CMBPol Study Team), *AIP Conf.Proc.* **1141**, 10 (2009), [arXiv:0811.3919 \[astro-ph\]](#).
- [11] P. Andre *et al.* (PRISM Collaboration), (2013), [arXiv:1306.2259 \[astro-ph.CO\]](#).
- [12] R. W. Ogburn *et al.*, in *Society of Photo-Optical Instrumentation Engineers (SPIE) Conference Series*, Vol. 8452 (2012) [arXiv:1208.0638 \[astro-ph.IM\]](#).
- [13] Z. Ahmed *et al.*, *Proc. SPIE* **9153**, 91531N (2014).
- [14] T. Matsumura *et al.*, *Proc. SPIE* **8452**, 84523E (2012).
- [15] B. A. Benson *et al.*, (2014), [arXiv:1407.2973 \[astro-ph.IM\]](#).
- [16] P. Oxley, P. Ade, C. Baccigalupi, P. deBernardis, H.-M. Cho, *et al.*, *Proc.SPIE Int.Soc.Opt.Eng.* **5543**, 320 (2004), [arXiv:astro-ph/0501111 \[astro-ph\]](#).
- [17] B. Crill, P. Ade, E. Battistelli, S. Benton, R. Bihary, *et al.*, (2008), [arXiv:0807.1548 \[astro-ph\]](#).
- [18] K. W. Masui and U.-L. Pen, *Phys.Rev.Lett.* **105**, 161302 (2010), [arXiv:1006.4181 \[astro-ph.CO\]](#).
- [19] L. Book, M. Kamionkowski, and F. Schmidt, *Phys.Rev.Lett.* **108**, 211301 (2012), [arXiv:1112.0567 \[astro-ph.CO\]](#).
- [20] T. L. Smith, H. V. Peiris, and A. Cooray, *Phys.Rev.* **D73**, 123503 (2006), [arXiv:astro-ph/0602137 \[astro-ph\]](#).
- [21] L. Boyle, K. M. Smith, C. Dvorkin, and N. Turok, (2014), [arXiv:1408.3129 \[astro-ph.CO\]](#).
- [22] M. Grana, *Phys.Rept.* **423**, 91 (2006), [arXiv:hep-th/0509003 \[hep-th\]](#).
- [23] M. R. Douglas and S. Kachru, *Rev.Mod.Phys.* **79**, 733 (2007), [arXiv:hep-th/0610102 \[hep-th\]](#).
- [24] F. Denef, M. R. Douglas, and S. Kachru, *Ann.Rev.Nucl.Part.Sci.* **57**, 119 (2007), [arXiv:hep-th/0701050 \[hep-th\]](#).
- [25] F. Denef (2008) pp. 483–610, [arXiv:0803.1194 \[hep-th\]](#).
- [26] N. Bartolo, S. Matarrese, and A. Riotto, *Phys.Rev.* **D64**, 123504 (2001), [arXiv:astro-ph/0107502 \[astro-ph\]](#).
- [27] D. Wands, N. Bartolo, S. Matarrese, and A. Riotto, *Phys.Rev.* **D66**, 043520 (2002), [arXiv:astro-ph/0205253 \[astro-ph\]](#).
- [28] A. R. Liddle, A. Mazumdar, and F. E. Schunck, *Phys.Rev.* **D58**, 061301 (1998), [arXiv:astro-ph/9804177 \[astro-ph\]](#).
- [29] P. Kanti and K. A. Olive, *Phys.Rev.* **D60**, 043502 (1999), [arXiv:hep-ph/9903524 \[hep-ph\]](#).
- [30] P. Kanti and K. A. Olive, *Phys.Lett.* **B464**, 192 (1999), [arXiv:hep-ph/9906331 \[hep-ph\]](#).
- [31] N. Kaloper and A. R. Liddle, *Phys.Rev.* **D61**, 123513 (2000), [arXiv:hep-ph/9910499 \[hep-ph\]](#).
- [32] R. Easther and L. McAllister, *JCAP* **0605**, 018 (2006), [arXiv:hep-th/0512102 \[hep-th\]](#).
- [33] S. Dimopoulos, S. Kachru, J. McGreevy, and J. G. Wacker, *JCAP* **0808**, 003 (2008), [arXiv:hep-th/0507205 \[hep-th\]](#).
- [34] S. A. Kim and A. R. Liddle, *Phys.Rev.* **D74**, 023513 (2006), [arXiv:astro-ph/0605604 \[astro-ph\]](#).
- [35] S. A. Kim and A. R. Liddle, *Phys.Rev.* **D76**, 063515 (2007), [arXiv:0707.1982 \[astro-ph\]](#).
- [36] R. Easther, J. Frazer, H. V. Peiris, and L. C. Price, *Phys.Rev.Lett.* **112**, 161302 (2014), [arXiv:1312.4035 \[astro-ph.CO\]](#).
- [37] D. Wenren, (2014), [arXiv:1405.1411 \[hep-th\]](#).
- [38] F. Vernizzi and D. Wands, *JCAP* **0605**, 019 (2006), [arXiv:astro-ph/0603799 \[astro-ph\]](#).
- [39] T. Battefeld and R. Easther, *JCAP* **0703**, 020 (2007), [arXiv:astro-ph/0610296 \[astro-ph\]](#).
- [40] S. A. Kim and A. R. Liddle, *Phys.Rev.* **D74**, 063522 (2006), [arXiv:astro-ph/0608186 \[astro-ph\]](#).

- [41] J. Frazer, *Journal of Cosmology and Astroparticle Physics* **2014**, 028 (2013), [arXiv:1303.3611 \[astro-ph.CO\]](#).
- [42] D. V. Hinkley, *Biometrika* **56**, 635 (1969).
- [43] M. J. Mortonson, H. V. Peiris, and R. Easther, *Phys.Rev.* **D83**, 043505 (2011), [arXiv:1007.4205 \[astro-ph.CO\]](#).
- [44] J. Martin, C. Ringeval, and R. Trotta, *Phys. Rev. D* **83**, 063524 (2011), [arXiv:1009.4157 \[astro-ph.CO\]](#).
- [45] R. Easther and H. V. Peiris, *Phys.Rev.* **D85**, 103533 (2012), [arXiv:1112.0326 \[astro-ph.CO\]](#).
- [46] J. Martin, C. Ringeval, R. Trotta, and V. Vennin, *JCAP* **1403**, 039 (2014), [arXiv:1312.3529 \[astro-ph.CO\]](#).
- [47] D. Salopek, J. Bond, and J. M. Bardeen, *Phys.Rev.* **D40**, 1753 (1989).
- [48] L. C. Price, J. Frazer, J. Xu, H. V. Peiris, and R. Easther, (2014), [arXiv:1410.0685 \[astro-ph.CO\]](#).
- [49] R. Easther and J. T. Giblin, *Phys.Rev.* **D72**, 103505 (2005), [arXiv:astro-ph/0505033 \[astro-ph\]](#).
- [50] A. Aazami and R. Easther, *JCAP* **0603**, 013 (2006), [arXiv:hep-th/0512050 \[hep-th\]](#).
- [51] L. Alabidi and D. H. Lyth, *JCAP* **0605**, 016 (2006), [arXiv:astro-ph/0510441 \[astro-ph\]](#).
- [52] Y.-S. Piao, *Phys.Rev.* **D74**, 047302 (2006), [arXiv:gr-qc/0606034 \[gr-qc\]](#).
- [53] D. I. Kaiser and E. I. Sfakianakis, *Phys.Rev.Lett.* **112**, 011302 (2014), [arXiv:1304.0363 \[astro-ph.CO\]](#).
- [54] R. Kallosh and A. Linde, *JCAP* **1307**, 002 (2013), [arXiv:1306.5220 \[hep-th\]](#).
- [55] R. Kallosh and A. Linde, *JCAP* **1310**, 033 (2013), [arXiv:1307.7938](#).
- [56] R. Kallosh and A. Linde, *JCAP* **1312**, 006 (2013), [arXiv:1309.2015 \[hep-th\]](#).
- [57] D. Sloan, (2014), [arXiv:1407.3977 \[gr-qc\]](#).
- [58] <http://www.nesi.org.nz>.